Supporting Information

Exploring the Thermoelectric Properties of Two-Dimensional Organic Conjugated Polymers with Dirac Cone-Like Electronic Structures

Jie Zhu,[a,b] Yajing Sun,[*a,b] Zhen Zhang, [*a] Wenping Hu[a,c]

[a] *Key Laboratory of Organic Integrated Circuits, Ministry of Education & Tianjin Key Laboratory of Molecular Optoelectronic Sciences, Department of Chemistry, School of Science, Tianjin University, Tianjin 300072, China.*

[b] *Haihe Lab of ITAI, Tianjin 300051, China.*

[c] *Joint School of National University of Singapore and Tianjin University, Fuzhou 350207, Fujian, China.*

[*]Corresponding author.

E-mail address: syj19@ tju.edu.cn (Y. Sun), zhzhen@tju.edu.cn(Z. Zhang)

Thermal Stability Simulation

We employed VASP for AIMD simulations at various temperatures to investigate the thermal stability of materials. During the calculations, the energy convergence threshold was set to 10^{-4} eV, and a 2×2×1 supercell was selected as the initial structure. The timestep was set to 2 fs, with a total simulation time of 3 ps[1,2].

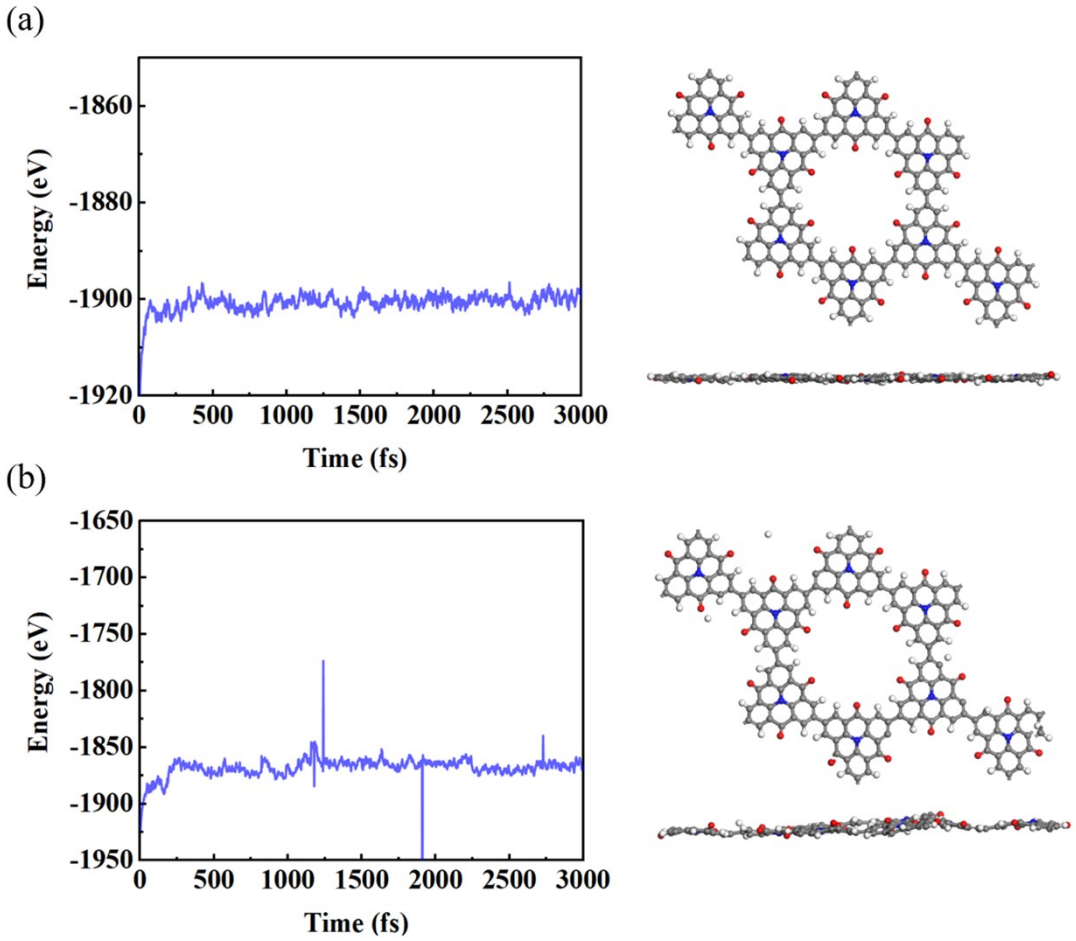

Figure S1. The total energy fluctuations of CTPA-polymer during AIMD simulation at (a) 500 K, (b) 700K (left). A snapshot of the crystal structure after 3000fs is provided (right).

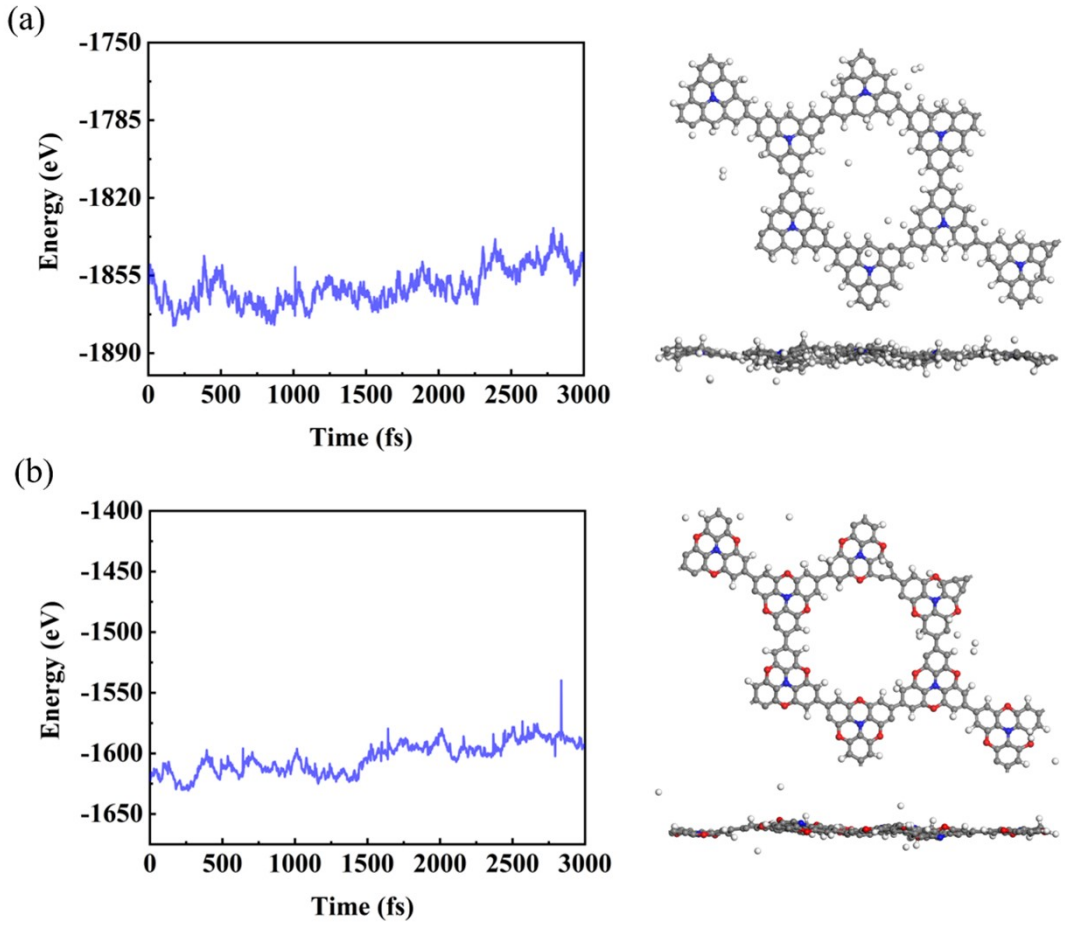

Figure S2. The total energy fluctuations of (a) MTPA polymer and (b) OTPA polymer during AIMD simulation at 300 K (left). A snapshot of the crystal structure after 3000fs is provided (right).

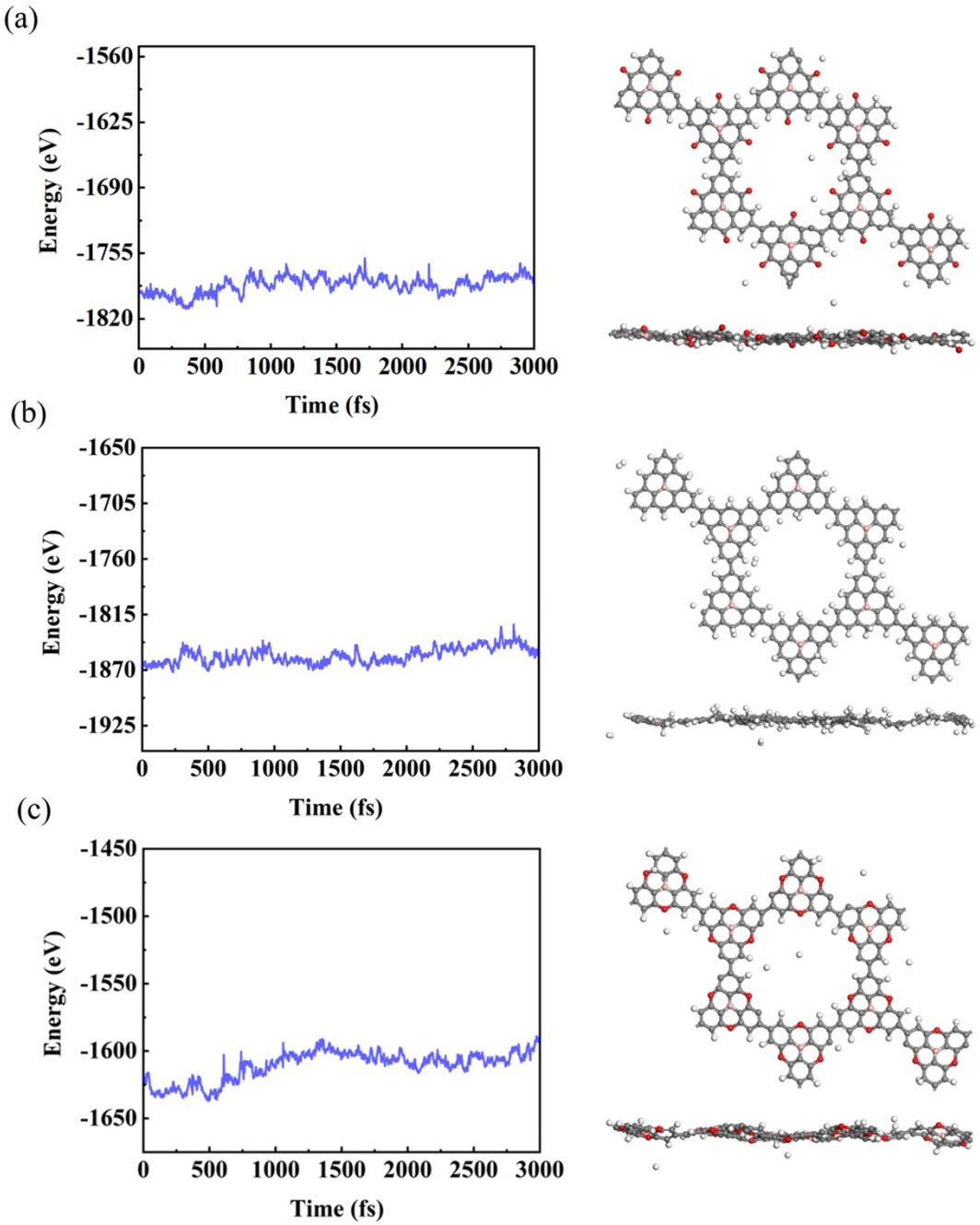

Figure S3. The total energy fluctuations of (a) CTPB-polymer, (b)MTPB-polymer and (c) OTPB-polymer during AIMD simulation at 300 K (left). A snapshot of the crystal structure after 3000fs is provided (right).

Electronic Structure and Charge Transport Properties

The electronic structure of the materials was improved using the Heyd-Scuseria-Ernzerhof hybrid functional (HSE06)[3,4].

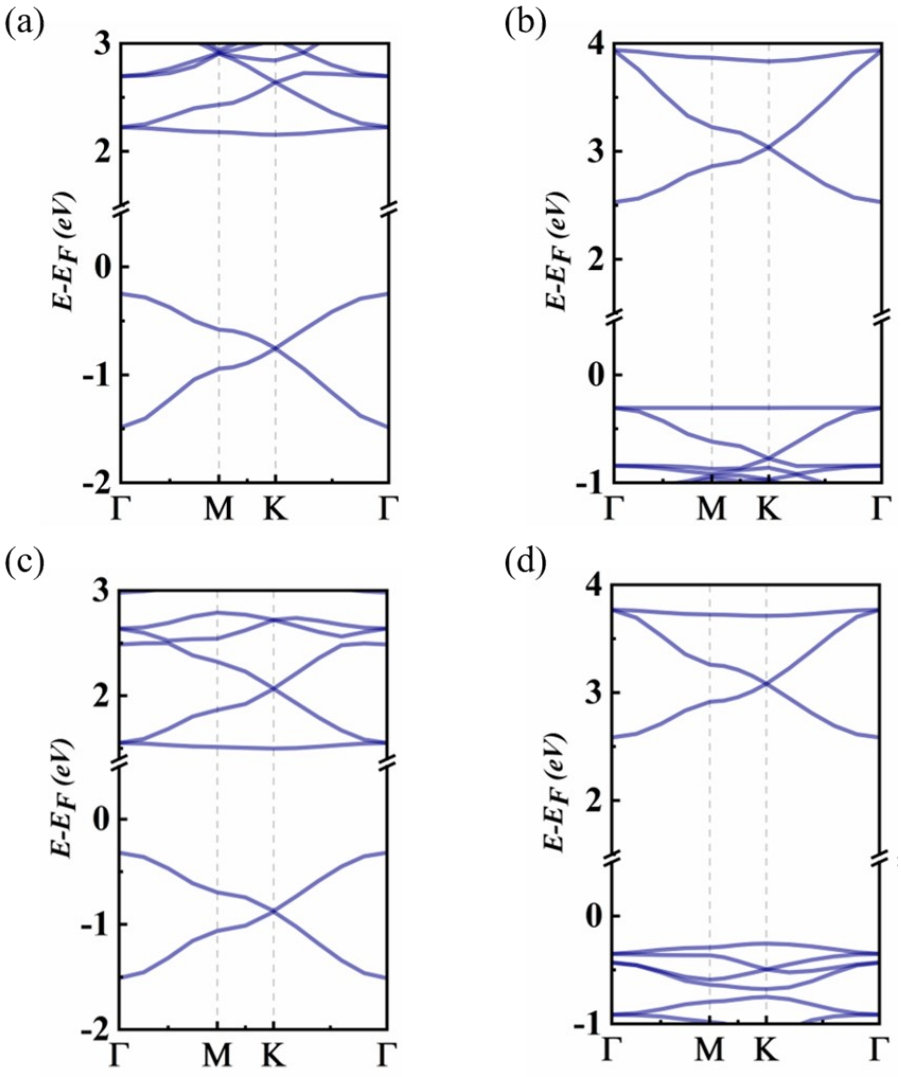

Figure S4. (a-d) Band structures of MTPA-polymer, MTPB-polymer, OTPA-polymer, and OTPB-polymer at the HSE06 level.

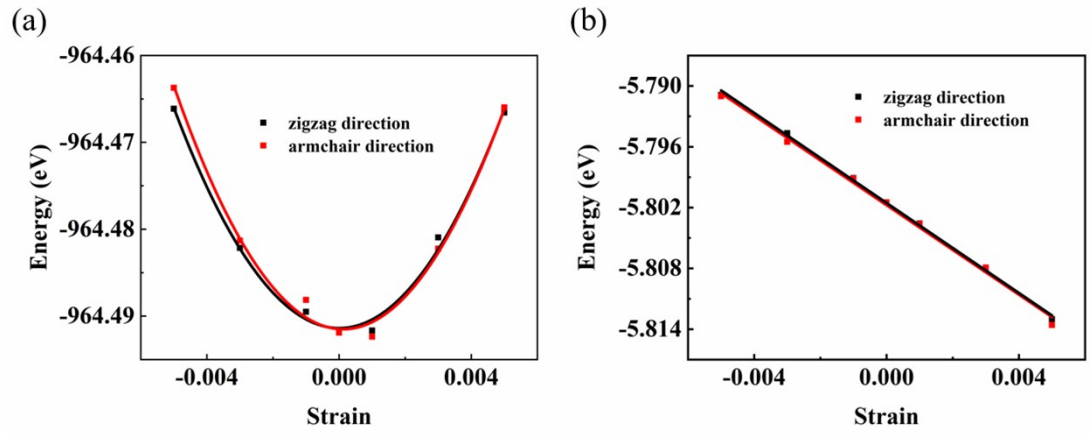

Figure S5. Simulation of CTPA-polymer carrier mobility[5,6]. (a) The functional relationship between total energy and strain under different strains along the zigzag and armchair directions. By simulating the change of total energy (E) with external uniaxial strain (δ) (where S_0 is the area of the optimized supercell), the in-plane stiffness C_{2D} of CTPA-polymer is obtained, defined as $\left[\partial^2 E/\partial\delta^2\right]/S_0$. (c) The variation of CTPA-polymer's conduction band minimum (CBM) with deformation in different directions.

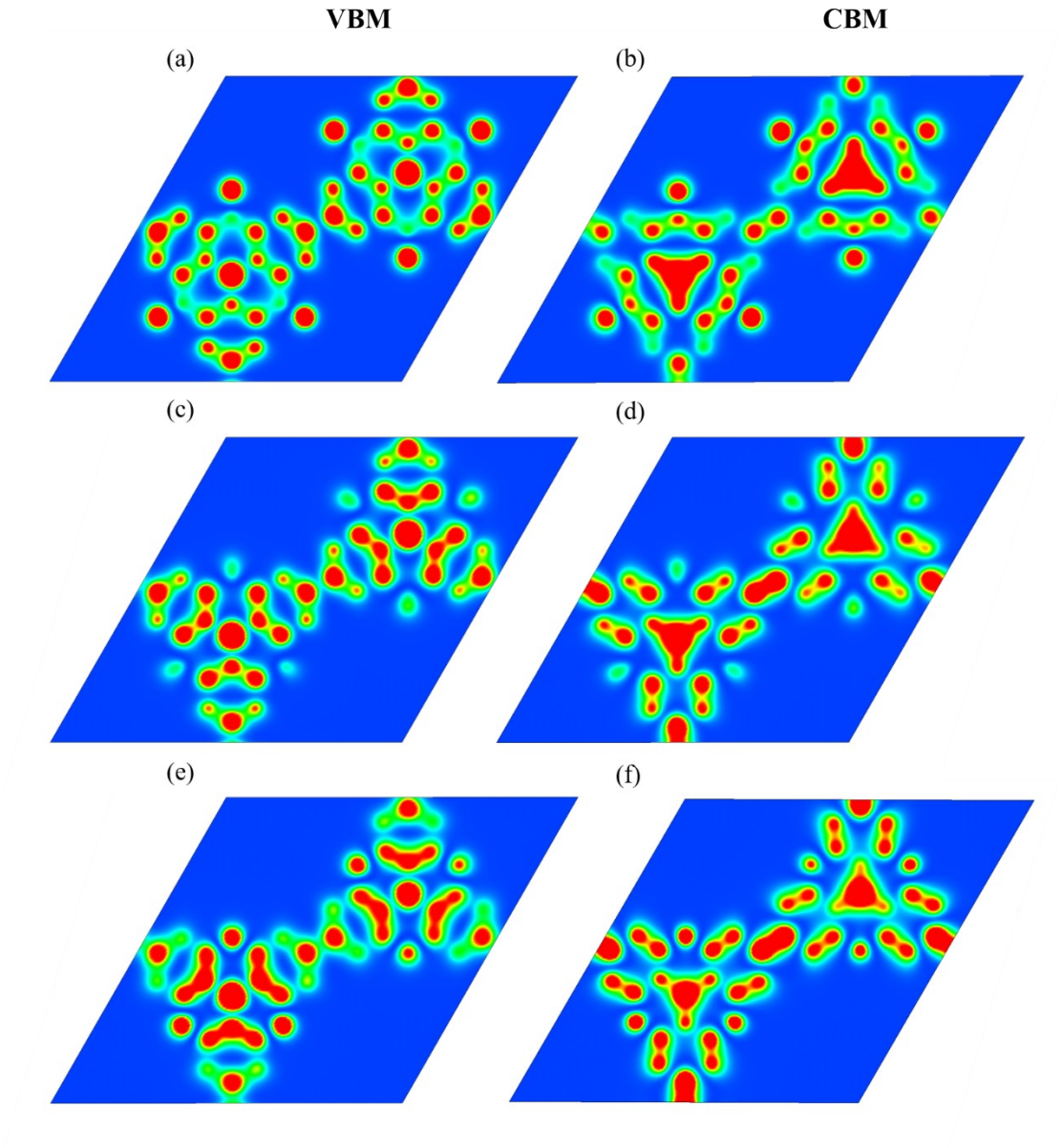

Figure S6. (a, c, e) Charge density distribution maps of the valence band maximum (VBM) for CTPA-polymer, MTPA-polymer, and OTPA-polymer, respectively. (b, d, f) Charge density distribution maps of the CBM for CTPB-polymer, MTPB-polymer, and OTPB-polymer, respectively.

Deep Neural Network Potential Energy Model

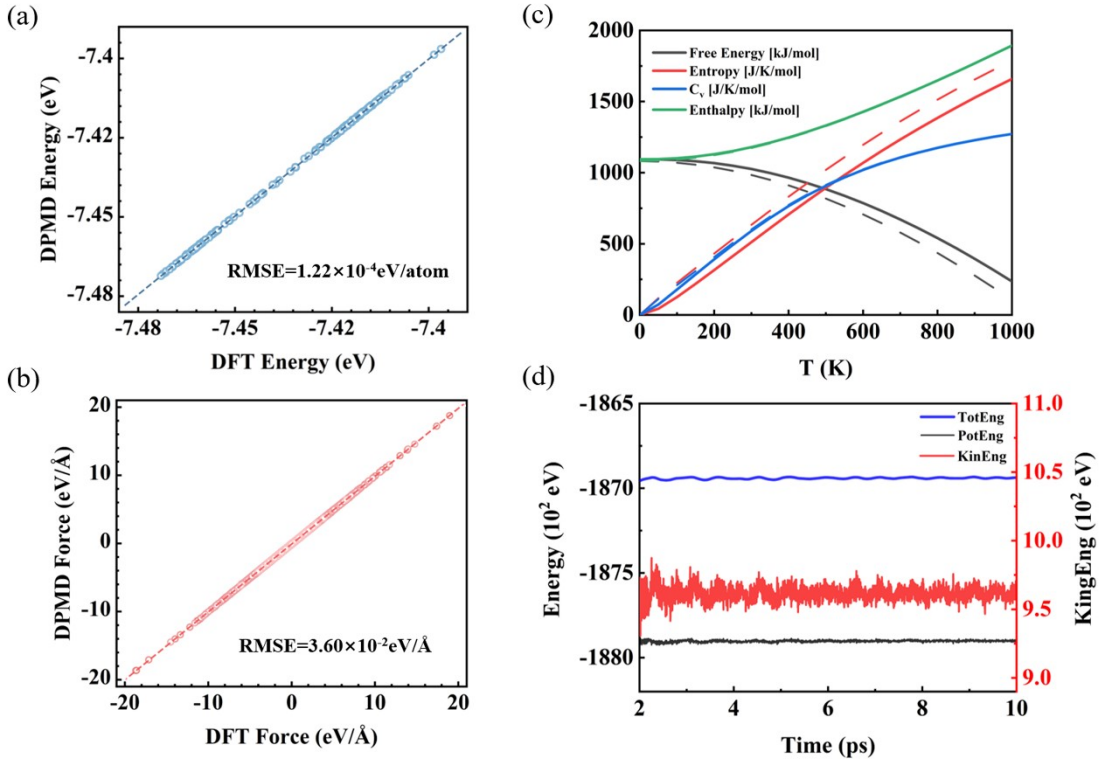

Figure S7. (a, b) Comparison between per-atom energy and atomic forces of CTPB-polymer calculated by DPMD and DFT. (c) Comparison of thermal properties (Helmholtz free energy, entropy, specific heat capacity, enthalpy) calculated by DPMD (dashed lines) and DFT (solid lines). (d) Energy variation of the CTPA-polymer at 300K under the NVT ensemble calculated by DPMD.

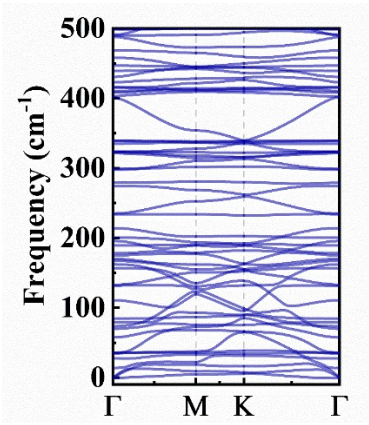

Figure S8. Phonon spectrum of CTPB-polymer calculated using DPMD.

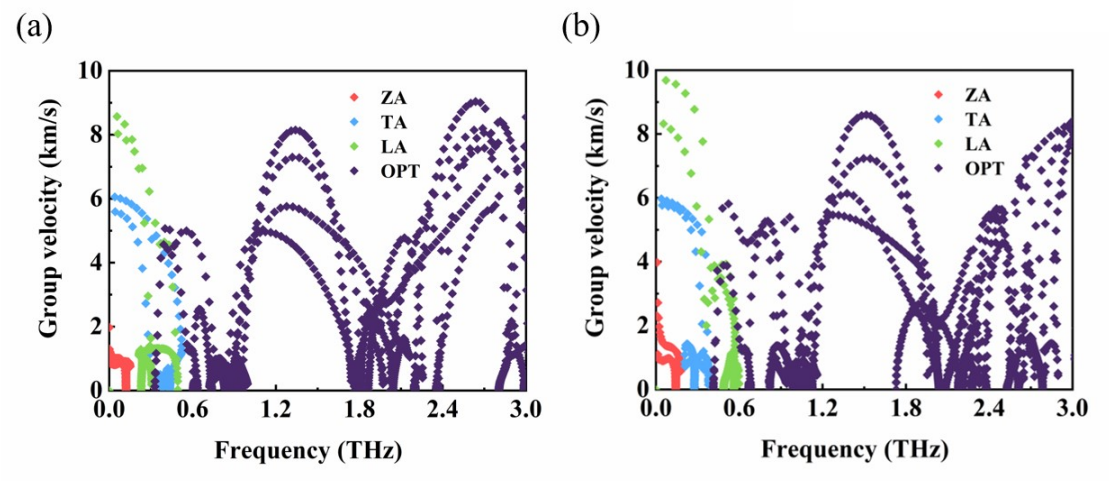

Figure S9. (a, b) Group velocities for CTPA-polymer and CTPB-polymer, respectively, as a function of frequency.

Lattice Thermal Conductivity

We obtained the thermal conductivity of CTPA-polymer through non-equilibrium molecular dynamics simulations using the Large-scale Atomic/Molecular Massively Parallel Simulator (LAMMPS) software[7]. We set up a heat bath and a cold bath in the middle and at both ends of the simulation domain, respectively, creating a stable temperature distribution, and predicted the thermal conductivity coefficient using Fourier's law, as illustrated in Figure S10a, which served as our computational domain.

Upon achieving a stable temperature gradient, we computed the thermal conductivity coefficient.

$$Q = -\kappa \frac{dT}{dx} \tag{1}$$

Here, Q denotes the rate of heat flux increase in the hot region and decrease in the cold region. The symbol κ stands for the thermal conductivity coefficient, and dT/dx represents the spatial and temporal average of the temperature gradient.

Considering the influence of the computational domain's size, particularly the dispersion of long-wavelength phonons in and around the heat source region[8,9], we extrapolated the values of thermal conductivity to the theoretical limit of an infinitely long system ($\kappa_1 \to \infty$). For system lengths that are comparable to or exceed the phonons' mean free path (λ), the interrelation between the reciprocal of the thermal conductivity coefficient and the reciprocal system length is established.

$$\frac{1}{\kappa(L)} = \frac{1}{\kappa_{L\to\infty}}\left(1 + \frac{\lambda}{L}\right) \tag{2}$$

To ascertain the thermal conductivities of CTPA-polymer and CTPB-polymer, we plotted the reciprocal of κ against the reciprocal of the computational domain length (L) along the heat flow direction, as illustrated in Figure S10b and c. This linear relationship was then extrapolated to $1/L \to 0$, allowing us to deduce the ultimate thermal conductivity values.

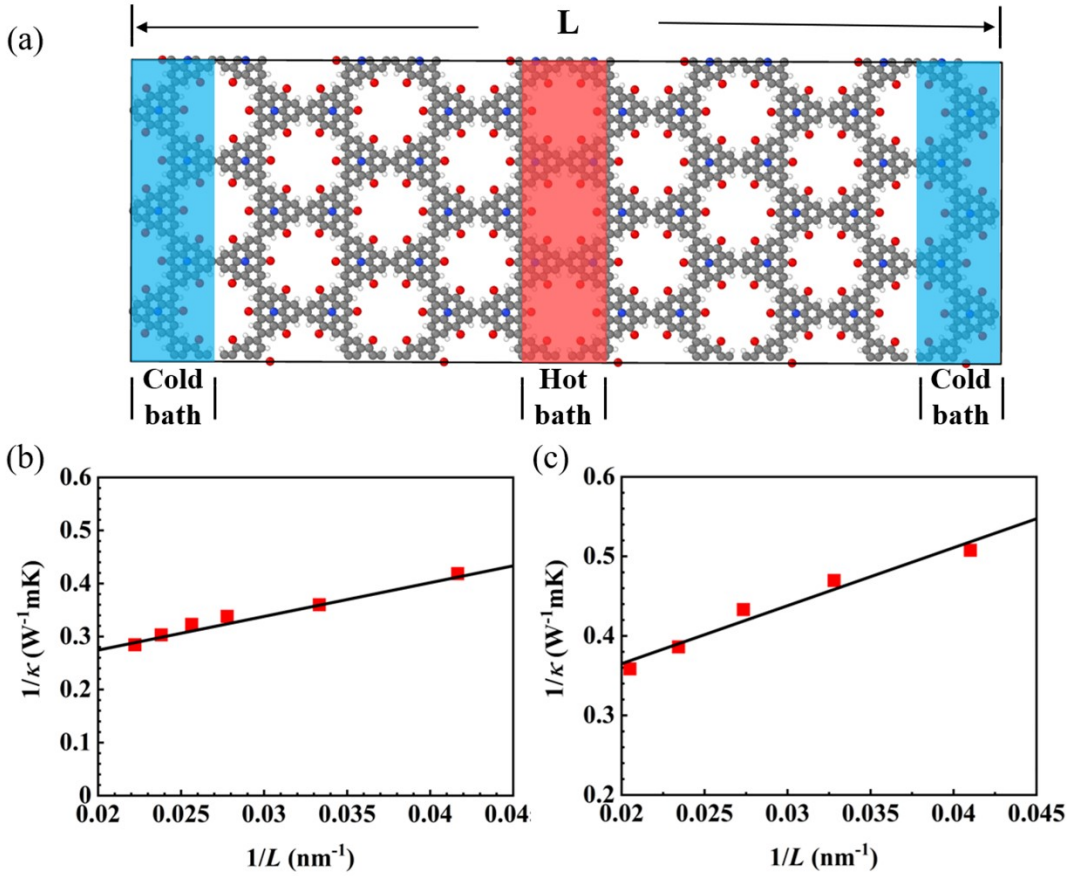

Figure S10. a) Illustration of the computational domain utilized for CTPA-polymer in NEMD simulations aimed at determining the in-plane thermal conductivity. (b, c) The inverse relationship of thermal conductivity coefficients, which are dependent on the size for CTPA-polymer and CTPB-polymer structures as determined by NEMD, plotted against the inverse of the length of the computational domain in the direction where heat is applied. The extrapolation of the linear fit to $1/L \rightarrow 0$ is used to forecast the overall thermal conductivity.

Thermoelectric Properties

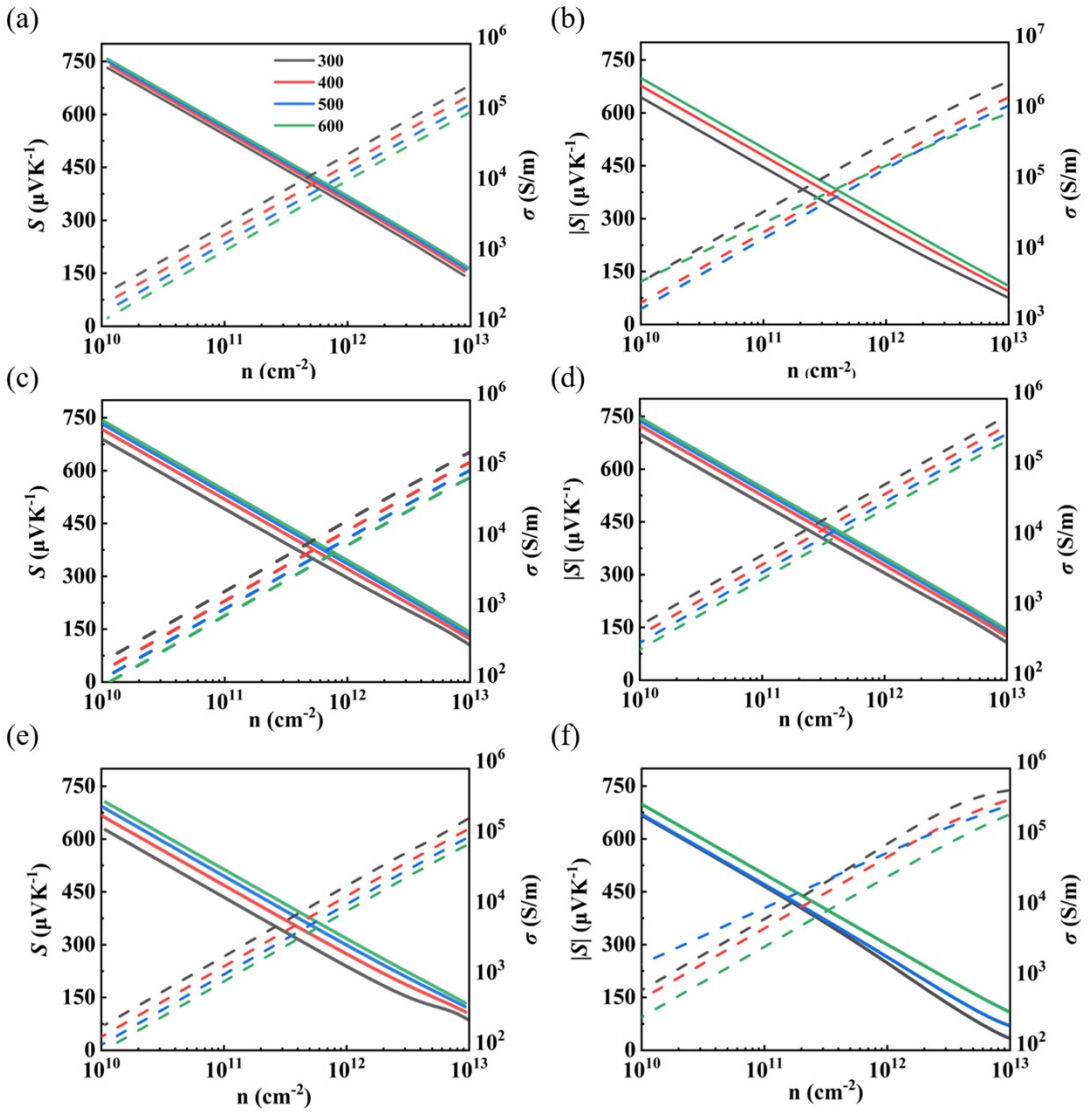

Figure S11. Variation of the Seebeck coefficient (S) and electrical conductivity (σ) with carrier concentration at different temperatures. (a-f) Correspond to CTPA-polymer, CTPB-polymer, MTPA-polymer, MTPB-polymer, OTPA-polymer, and OTPB-polymer, respectively.

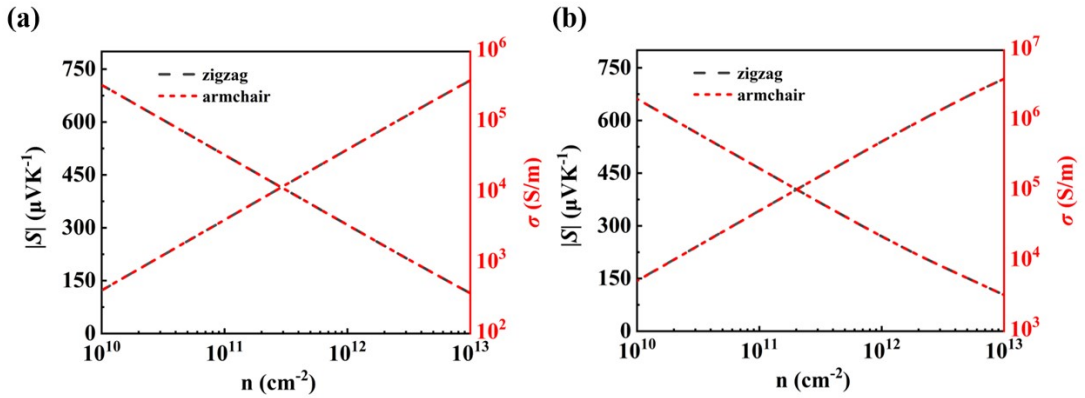

Figure S12. Changes in S and σ of (a) CTPA-polymer and (b) CTPB-polymer in different directions as a function of carrier concentration at 300K.

Bipolar Thermoelectric Properties of CTPA-CTPB Heterojunction

The heterostructure was constructed by stacking CTPA-polymer and CTPB-polymer monolayers in an AA fashion. Through convergence tests and structural optimization, we obtained a unit cell with an interlayer distance of 3.74Å and a lattice constant of 17.45Å.

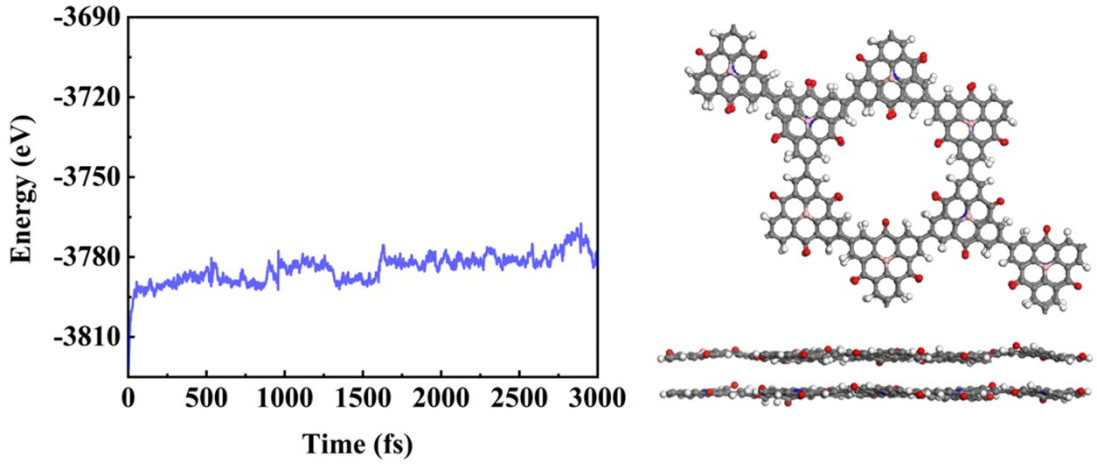

Figure S13. The total energy fluctuations of CTPAB-polymer during AIMD simulation at 300 K (left). A snapshot of the crystal structure after 3000 fs is provided (right).

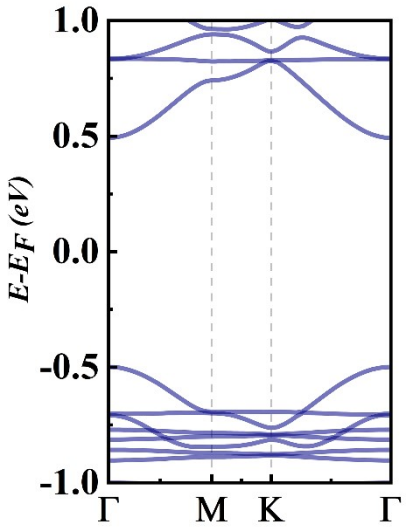

Figure S14. Band structure of CTPAB-polymer at the PBE level.

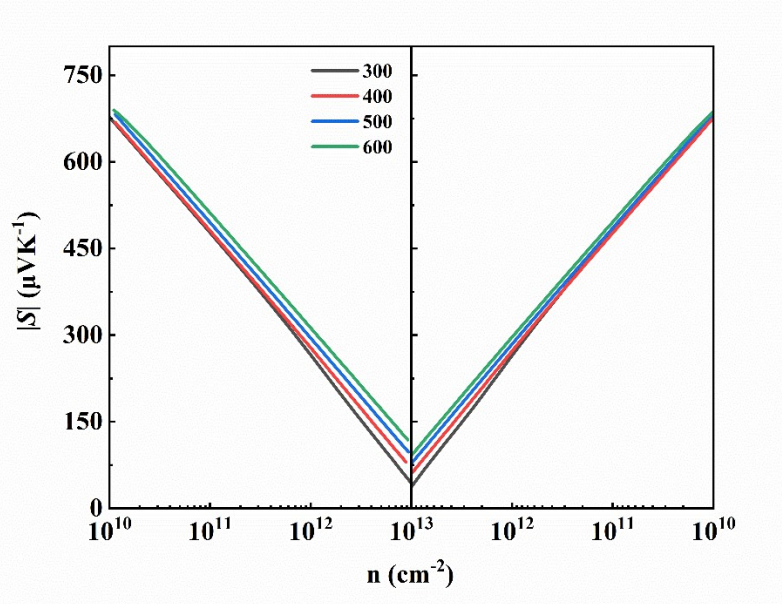

Figure S15. Variation of *S* with carrier concentration at different temperatures for CTPAB-polymer, with the left side of each graph representing p-type thermoelectric performance and the right side representing n-type thermoelectric performance.

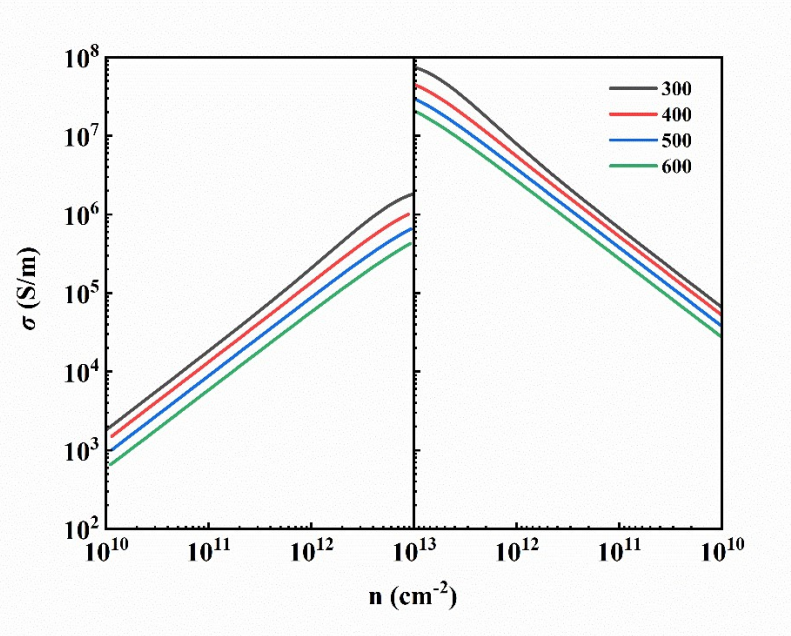

Figure S16. Variation of σ with carrier concentration at different temperatures for CTPAB-polymer, with the left side of each graph representing p-type thermoelectric performance and the right side representing n-type thermoelectric performance.

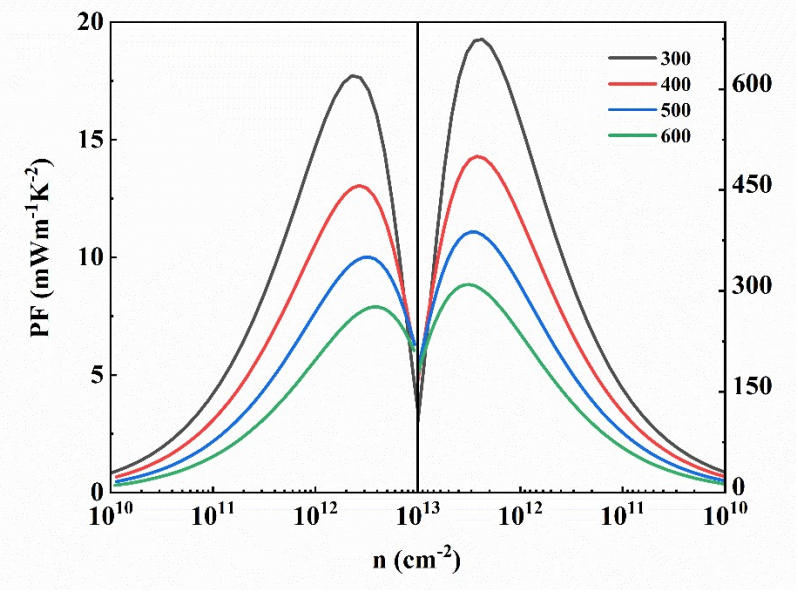

Figure S17. Variation of PF with carrier concentration at different temperatures for CTPAB-polymer, with the left side of each graph representing p-type thermoelectric performance and the right side representing n-type thermoelectric performance.

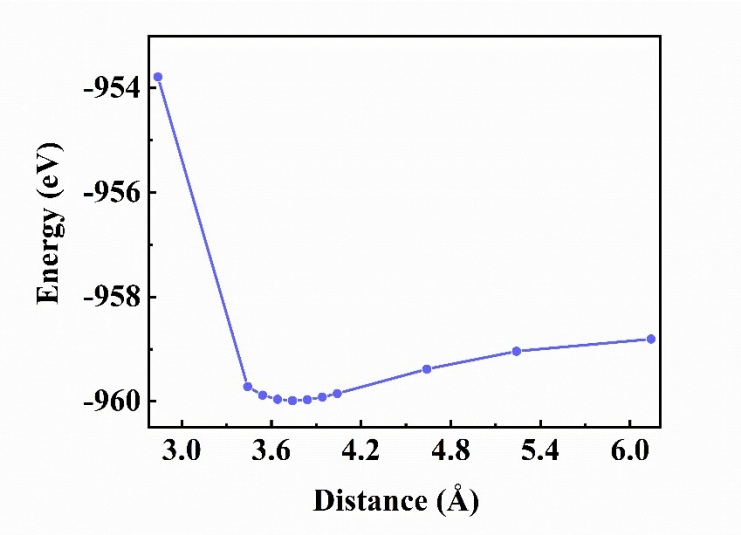

Figure S18. Curve of the total energy of the CTPAB-polymer system as a function of interlayer distance.

References

1 G. Qin, Q.-B. Yan, Z. Qin, S.-Y. Yue, M. Hu and G. Su, *Phys. Chem. Chem. Phys.*, 2015, **17**, 4854–4858.

2 P. E. Blöchl and M. Parrinello, *Phys. Rev. B*, 1992, **45**, 9413–9416.

3 L. Kronik and J. B. Neaton, *Annu. Rev. Phys. Chem.*, 2016, **67**, 587–616.

4 A. F. Izmaylov and G. E. Scuseria, *J. Chem. Phys.*, 2008, **129**, 034101.

5 M. D. Siao, W. C. Shen, R. S. Chen, Z. W. Chang, M. C. Shih, Y. P. Chiu and C.-M. Cheng, *Nat Commun*, 2018, **9**, 1442.

6 J. Bardeen and W. Shockley, *Phys. Rev.*, 1950, **80**, 72–80.

7 S. Plimpton, *J. Comput. Phys.*, 1995, **117**, 1–19.

8 P. K. Schelling, S. R. Phillpot and P. Keblinski, *Phys. Rev. B*, 2002, **65**, 144306.

9 P. Jund and R. Jullien, *Phys. Rev. B*, 1999, **59**, 13707–13711.